This is an author-created version for self-archiving
The final version, published in Journal of the Mechanics and Physics of Solids, Vol. 63, February 2014, Pages 201−213, is available at:
http://www.sciencedirect.com
http://dx.doi.org/10.1016/j.jmps.2013.09.009.
doi:10.1016/j.jmps.2013.09.009

Size-dependence of the dielectric breakdown strength from nano- to millimeter scale

By Claudia Neusel and Gerold A. Schneider*

Institute of Advanced Ceramics, Hamburg University of Technology, Denickestraße 15, 21073 Hamburg, Germany

[*] Corresponding-Author: Prof. Gerold A. Schneider
Tel: +49-(0)40 42878 -3037
Fax: +49-(0)40 42878 -2647
E-mail: g.schneider@tuhh.de; g.schneider@tu-harburg.de

Keywords: dielectric breakdown strength, size-dependence, dielectric breakdown toughness, ceramics, polymers

Abstract

Dielectric breakdown decisively determines the reliability of nano- to centimeter sized electronic devices and components. Nevertheless, a systematic investigation of this phenomenon over the relevant lengths scales and materials classes is still missing. Here, the thickness and permittivity-dependence of the dielectric breakdown strength of insulating crystalline and polymer materials from the millimeter down to the nanometer scale is investigated. While the dependence of breakdown strength on permittivity was found to be thickness-independent for materials in the nm-mm range, the magnitude of the breakdown strength was found to change from a thickness-independent, intrinsic regime, to a thickness-dependent, extrinsic regime. The transition-thickness is interpreted as the characteristic length of a breakdown-initiating conducting filament. The results are in agreement with a model, where the dielectric breakdown strength is defined in terms of breakdown toughness and length of a conducting filament.

1. Introduction

Since about 90 years the phenomenon of dielectric breakdown is investigated theoretically and experimentally. Dielectric breakdown is a limiting factor for the reliability of nano- to millimeter or centimeter-sized electronic devices and components (O'Dwyer 1958, Nafría et al. 1996, Dissado and Fothergill 1992). First theories to describe the mechanism of dielectric breakdown as an electron avalanche were developed by von Hippel (1931a, b, 1932), Fröhlich (1939) and O'Dwyer (1967). Within the same time the idea of a thermal breakdown mechanism came up (e.g. Fock 1927, Moon 1931 and Wagner 1948). These two basic breakdown models were later on refined for specific applications like thin films by e.g. Klein and Gafni (1966) and enhanced by e.g. O'Dwyer (1982) or Budenstein (1980). Stark and Garton (1955) developed an electromechanical breakdown model for thermoplastic polymers which later on was modified by Fothergill (1991) to a filamentary electromechanical breakdown model. The filamentary electromechanical breakdown model as well as the electro-fracture mechanics model of Zeller and Schneider (1984) based on concepts of fracture mechanics. The analogy between fracture mechanics and dielectric breakdown was also taken into account for models developed by e.g. McMeeking (1986), Suo (1993), Vojta and Clarke (1998), Fu et al. (2000), Wang and Zhang (2001), Zhang and Gao (2004), Beom and Kim (2008), Lin et al. (2009) and Schneider (2013). Whereas electron avalanche breakdown models are appropriate for thin films, gate oxides and other submicron-sized electronic devices, continuum theoretical models are necessary for macroscopic high voltage components like for example X-ray tubes, spark plugs, high-voltage cables or switches. Recently Sun et al. (2012, 2013) showed convincingly that density function perturbation theory calculations (DFPT) based on von Hippels avalanche model are able to predict the intrinsic breakdown for covalently bonded and ionic materials.

Given the fact that the phenomenon of dielectric breakdown covers the lengths scale range from centimeter to nanometers, astonishingly there is no comprehensive study investigating its size-dependence over these lengths scales. Typically size-dependent measurements cover thicknesses over one or two orders of magnitude (e.g. Owate and Freer 1988, 1898, 1990, 1991, Malec et al. 2010). But there is no systematic study published, where the dielectric breakdown strength of different ceramic and polymer materials with relative permittivities from approximately 2 - 2000 over a thickness range from 2 nm - 2 mm are investigated.

The objective of this study is, to determine the size and permittivity-dependence of the breakdown strength of different insulating materials from the millimeter to the nanometer scale, and to identify the transition between a thickness-dependent to a thickness-independent

regime. Such a transition region had been shown by Joffé (1927) for glass and mica, but was not systematically investigated for other materials. To achieve this goal, existing data from the literature were collected and added to own measurements in size or permittivity regimes, which were not covered. It will be shown that there exists a transition-thickness from a thickness-independent, termed intrinsic, to a thickness-dependent, termed extrinsic, breakdown regime for the investigated materials. For an application in an electrical component, the knowledge of the transition-thickness enables to decide whether an intrinsic avalanche-type model has to be applied for the theoretical description of the breakdown or whether a macroscopic continuum model is necessary.

Focusing on bulk samples (> 1 μm), the experimental data basis is used to check the validity of a recently developed Griffith-type dielectric breakdown model (Schneider 2013). Existing models, like the avalanche breakdown model, thermal breakdown model or electromechanical breakdown model do not describe the measured thickness-dependence respectively permittivity-dependence. The Griffith-type dielectric breakdown model assumes tiny, electrically conducting filaments at the surface of the samples (Fig. 1a). When a critical electrical energy release rate is reached, the longest of these conducting filaments grows unstably to form the typical breakdown channel (Fig. 1b). This critical energy release rate, named the dielectric breakdown toughness, determines vice versa the dielectric breakdown field, if the conducting filament-length is known. Until now, the length and diameter of these conducting filaments is not known. In this investigation, the transition-thickness between extrinsic to intrinsic breakdown regime will be used, to estimate the initial length of breakdown-initiating conducting filament. As a consequence, the dielectric breakdown toughness can be calculated. This approach is very similar to mechanical brittle fracture, where small cracks are assumed to be present in the material. Upon mechanical loading, the energy release rate for a crack reaches a critical value, which may result in unstable crack growth and fracture of the material. Also in the mechanical case, the transition from a thickness-independent to a thickness-dependent regime is used to estimate the length of the failure-initiating cracks (Gao et al. 2003).

a) b)

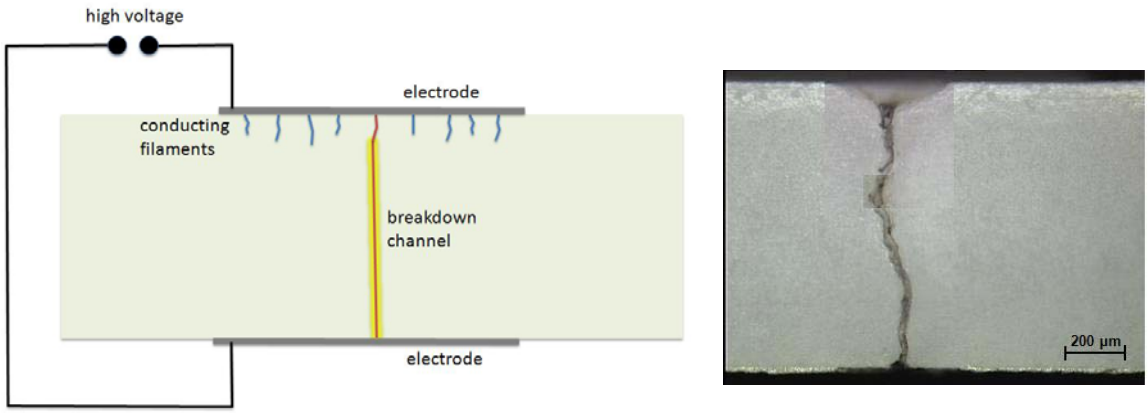

Fig. 1: a) Schematic picture of the dielectric breakdown initiated by conducting filaments. b) Light-microscopy image of a cross-section through an Al_2O_3 sample with a breakdown channel.

2. Materials and methods

2.1. Ceramic sample preparation

Dielectric breakdown tests were performed on ceramic samples with different thicknesses d and relative permittivities ε_r. Therefor cylindrical polycrystalline Al_2O_3-, TiO_2- and $BaTiO_3$-samples with a diameter of 28 mm were prepared.

All polycrystalline samples were formed using uniaxial- and cold-isostatic dry pressing and sintered in a chamber furnace in air (for more details see Table 1). After sintering the samples were ground plan-parallel to thicknesses in the range of 0.3-2 mm. Sample thicknesses in the range of 0.7-0.24 mm were prepared by cutting grooves of different depth into 0.3 mm thick samples with a precision cutting machine (Exakt Apparatebau GmbH & Co.KG, Germany).

In order to extend the variety of relative permittivities, {110}-oriented $SrTiO_3$ single crystals grown by the flame fused method (Crystal GmbH and Co.KG, Berlin) were tested. The squared $SrTiO_3$ single crystals had an edge length of 20 mm and a thickness of 0.3 mm.

Tab. 1: Processing steps of Al_2O_3-, TiO_2- and $BaTiO_3$-samples.

	Al_2O_3	**TiO_2**	**$BaTiO_3$**
Powder	Taimicron TM-DAR 99.99% pure Krahn Chemie GmbH, Hamburg	14027 TiO_2 extra pure Riedle de Häen AG, Seelze	$BaTiO_3$ 99.7% pure Alfa Aesar GmbH Co KG, Karlsruhe
Unidirectional pre-pressing	8.5 MPa	8.5 MPa	8.5 MPa
Bidirectional pressing	17 MPa	17 MPa	17 MPa
Cold-isostatic pressing	150 MPa	150 MPa	150 MPa
Sintering cycle	10 K/min 1350°C 1h 10 K/min 40°C	3 K/min 1550°C 2h 10 K/min 40°C	3 K/min 1400°C 2h 10 K/min 40°C

2.2. Ceramic sample characterization

After sintering, polishing and thermal etching the density and grain size of the samples were evaluated according to the Archimedes and mean intercept length method. The relative permittivities were measured with 1 V in the range of 20 Hz-1 MHz with a LCR meter (HP 4284 A, Hewlett-Packard, Japan). For this, the sample surface was painted with conductive silver and connected via two copper wires, one on each side, to a test fixture (HP 16047 A). In Table 2 the measured densities, grain sizes and relative permittivities are summarized.

Tab. 2: Characterization of Al_2O_3-, TiO_2-, $SrTiO_3$- and $BaTiO_3$-samples.

	Density [g/cm^3]	**Grain size [µm]**	**Relative permittivity at (1 kHz)**
Al_2O_3	3.9	1	7
TiO_2	4.1	3	109
$SrTiO_3$	5.1 [a]	single crystal [a]	330
$BaTiO_3$	5.6	25	1599

[a] According data sheet Crystal GmbH, Berlin, Germany.

2.3. Polymer preparation and characterization

Polymer thin films were prepared via spin coating process. Solutions of Poly-(methyl methacrylate) (PMMA) and 2-butanone respectively polystyrene (PS) and n-butyl acetate with varying amounts of polymer were prepared. The amount of polymer in the solution was 2, 5, 10 and 15 wt% for PMMA and 5, 10 and 15wt% for PS. After dissolving the polymer, the solution was filtered with a 0.2 µm injection filter to remove particle contamination. In order to realize different film thicknesses, the spin parameters were varied from 1000 to 7000 rpm in 1000 rpm-steps. The spinning time was kept constant 45 s. Film thicknesses in the range of 200 – 4000 nm were reached. The film thicknesses were measured with a profilometer (DekTac 3030, Veeco Instruments Inc., USA). The polymer solutions were spin coated onto an indium tin oxide-(ITO) coated soda lime glass, which was used as substrate. The ITO-coating, as well as the second gold electrode sputtered onto the polymer film, served as electrodes for dielectric breakdown testing.

As bulk polymer material, commercially available PVC of 1 mm thickness was ground to thicknesses of 0.5 and 0.2 mm.

2.4. Dielectric breakdown test of thick ceramic and polymer samples

Dielectric breakdown tests were performed by a rectified ac high voltage signal and by a dc high voltage signal. The rectified ac voltage signal was realized by the formation of a 50 Hz voltage pulse via a function generator (Agilent 33220 A, Agilent Technologies, Inc., USA), which was further on stepwise amplified to high voltage by vacuum tubes, inductors and a transformer coil. Details of the high voltage amplifier are described in (Neusel et al. 2012). Al_2O_3 and TiO_2 samples in the range of 0.5-2 mm thickness and PVC samples of 0.2-1 mm thickness were tested using the rectified ac-voltage. The $BaTiO_3$-samples could not be tested using a rectified ac voltage signal because the maximum possible applied voltage was limited to a certain level. It is assumed that this is related to the ferroelectric domain switching behavior of $BaTiO_3$. Hence, a dc signal was applied which was generated by a dc high voltage generator HCN 140-35000 (F.u.G. Elektronik GmbH, Germany) with a maximum voltage of 35 kV. To ensure the comparability of dielectric breakdown strength values between $BaTiO_3$ and Al_2O_3 and TiO_2 despite the different voltage signals, 0.07–0.3 mm thick Al_2O_3 and 0.3 mm thick TiO_2 samples were tested using the dc high voltage generator HCN 140-35000 (F.u.G. Elektronik GmbH, Germany). Additionally 1 mm thick Al_2O_3 and TiO_2 samples were

tested using the dc high voltage generator ER75P4 (Glassman high voltage Inc., UK), which can generate a maximum high voltage signal of 75 kV. In Table 3 the high voltage signals used for different samples and thicknesses are summarized.

Tab. 3: Applied signal for dielectric breakdown test of Al_2O_3-, TiO_2- $SrTiO_3$ and $BaTiO_3$-samples and PVC.

	Thickness ≤ 0.3 mm	**Thickness > 0.3-1.7 mm**	**Thickness = 1 mm**
Al_2O_3	dc signal (HCN 140-35000)	rectified ac signal	dc signal (ER75P4)
TiO_2	dc signal (HCN 140-35000)	rectified ac signal	dc signal (ER75P4)
$SrTiO_3$	dc signal (HCN 140-35000)	-	-
$BaTiO_3$	dc signal (HCN 140-35000)	dc signal (HCN 140-35000)	-
PVC	rectified ac signal	rectified ac signal	-

Before performing the breakdown test, a circular layer of conductive silver was deposited onto the surface of all bulk ceramic and polymer samples to ensure a good electric connection between sample and electrodes. Afterwards, the samples were dried at 100°C for 5 h in a furnace to evaporate the solvent.

For the breakdown test, the samples were clamped between the electrodes. The high voltage signal was increased in 0.2 kV/s-steps for the dc and rectified ac signal, until the sample underwent dielectric breakdown characterized by a collapsing voltage signal. The maximum voltage directly before the collapse was defined as breakdown voltage V_{bd}.

In the case of the dc high voltage generator HCN 140-35000 a current limit of 4 mA and in the case of the dc high voltage generator ER75P4 a current limit of 2 mA was set. These currents were the maximum currents, which flow through the sample respectively through the channel, when breakdown occurs. As both generators indicate the achievement of the current limits, it was also used as indication that breakdown occurred. Both, dc and rectified ac breakdown tests were performed in silicon oil at room temperature using the same measuring cell (Neusel et al. 2012). The high voltage electrode of the cell, connected to the high voltage

source, was designed as brass-made pin electrode with rounded tip, enclosed by a PVC cylinder to prevent flashover behavior. For Al_2O_3 and TiO_2 samples thicker than 0.3 mm and all PVC samples a ground electrode made of stainless steel with a flat surface area similar to a Rogowski profile was used (Fig. 2a). In order to reduce weight onto the fragile 0.3 mm and smaller Al_2O_3, TiO_2, and $SrTiO_3$ samples the ground electrode was exchanged from Rogowski profile to a pin electrode (Fig. 2b). All $BaTiO_3$ samples were tested using the pin to pin electrode configuration (Fig. 2b).

a) b)

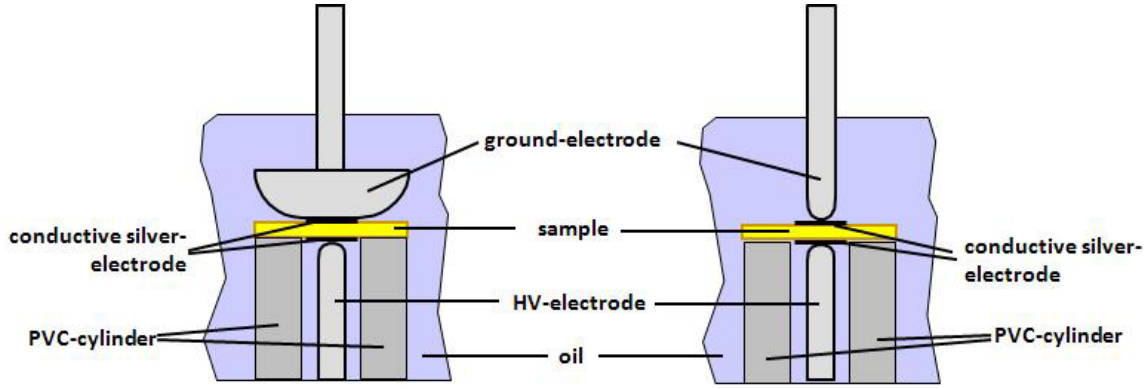

Fig. 2: Schematic picture of the electrode configuration used for breakdown tests of a) samples > 0.3 mm and b) samples 0.07mm-0.3 mm.

2.5. Dielectric breakdown test of polymer thin films

The dielectric breakdown test on polymer thin films was performed at room temperature using a dc voltage signal generated by a High-Resistance Meter (Agilent 4339B, Agilent Technologies, Inc., USA). At one edge of the substrate the polymer thin film was removed to connect the ITO-electrode via conductive silver and a wire with the voltage generator (Fig. 3). The second electrode was connected to the voltage generator with a spherical electrode, which was pressed onto the sputtered gold electrode with a force of 0.07 N. The voltage signal was stepwise increased in approx. 0.2 V/s-steps. As the Agilent 4339B High-Resistance Meter is able to measure currents in the range of 60 fA-500 mA, dielectric breakdown of the film was defined as sudden current increase above 500 mA.

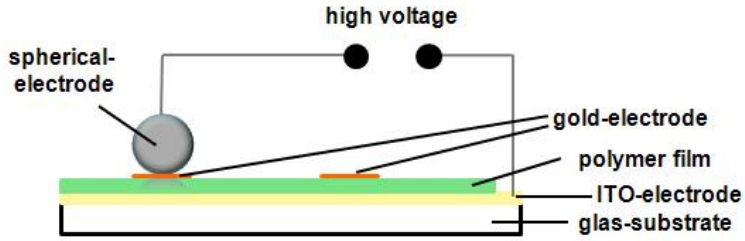

Fig. 3: Schematic side-view of the electrode configuration for breakdown tests on thin films.

3. Results and Discussion

3.1. Breakdown strength from nano to millimeter scale

Fig. 4 shows the results of the measured breakdown strength E_{bd}, defined as breakdown voltage V_{bd} per sample thickness d, versus sample thickness d in the range from 2 mm to 2 nm. All investigated samples showed single breakdown channels as failure phenomenon. Added are also literature data to cover the whole thickness range. A thickness-dependent behaviour with $\frac{1}{\sqrt{d}}$-dependence as well as a thickness-independent regime is clearly visible. The thickness-independent regime is named intrinsic and attributed to the materials inherent maximum breakdown strength. On the other hand, the thickness-dependent regime is termed extrinsic and will be explained in more detail in Section 3.4. The transition-thickness d_t between the extrinsic and intrinsic regime is approx. between 1 µm and 20 µm. It cannot be determined more precisely with the existing data, which almost cover 6 orders of magnitude in lengths.

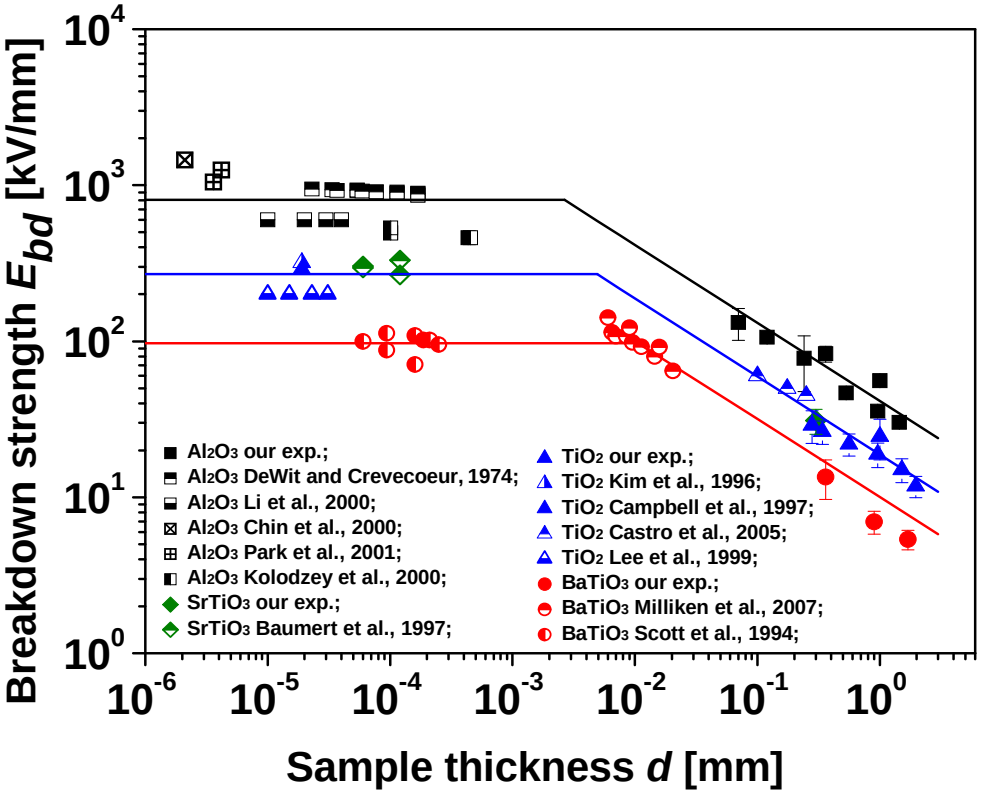

Fig. 4: Double logarithmic plot of measured dielectric breakdown strength E_{bd} versus sample thickness d for Al_2O_3, TiO_2, $SrTiO_3$ and $BaTiO_3$. The data points which were taken from literature sources are labeled with their reference number in parentheses. The marked lines in the range of constant breakdown strengths are fitted as mean values. In the range of thickness-dependent breakdown strength the marked lines are least square fits with a slope of -0.5.

A thickness-dependent evaluation of the investigated polymers between 2 mm and 200 nm is shown in Fig. 5. The breakdown strengths of PMMA, PS, PVC and PE show $\frac{1}{\sqrt{d}}$-dependence in the extrinsic breakdown regime and a transition to thickness-independent intrinsic breakdown strength. Even though the dielectric breakdown strengths of the investigated polymers are similar to the ceramic materials, the transition to the thickness-independent breakdown strength regime is almost an order of magnitude higher (d_t = 10 – 100 µm).

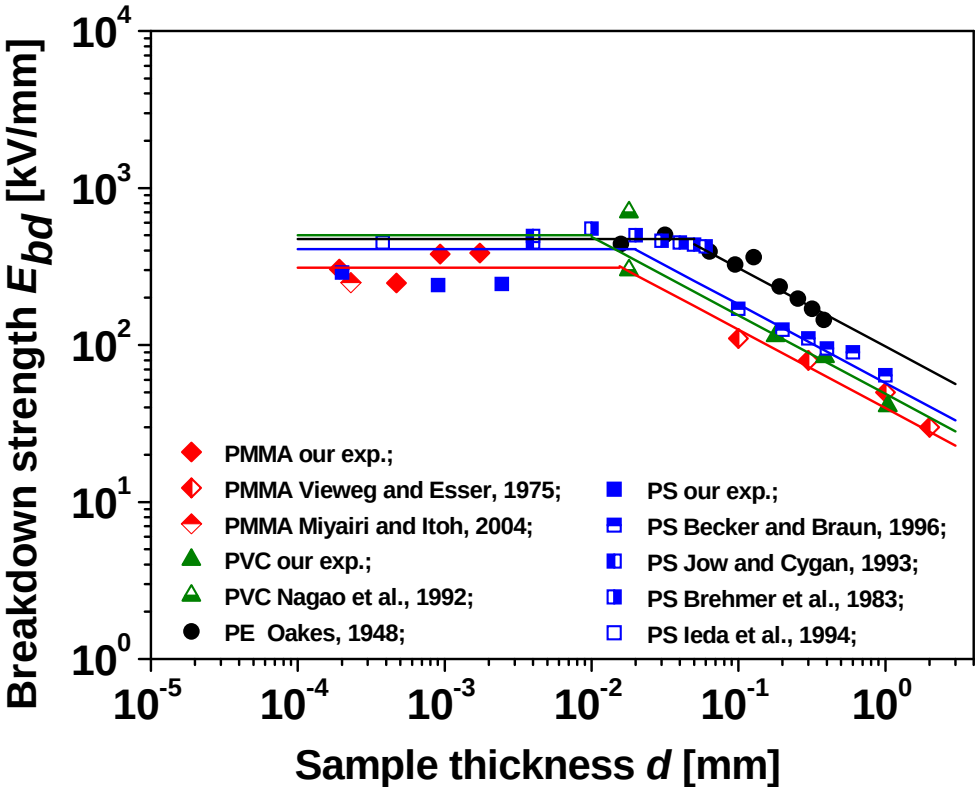

Fig. 5: Double logarithmic plot of measured dielectric breakdown strength E_{bd} versus sample thickness d for PMMA, PS, PVC and PE. The data points which were taken from literature sources are labeled with their reference number in parentheses. The marked lines in the range of constant breakdown strengths are fitted as mean values. In the range of thickness-dependent breakdown strength the marked lines are least square fits with a slope of -0.5.

The data plotted in Figs. 4 and 5 are from our experiments and from literature. Therefore, the sample preparation and voltage loading differs in the experiments. Nevertheless, the overall trend of a $\frac{1}{\sqrt{d}}$ -dependence is obvious. There is most probably an influence of the surface roughness, electrode geometry, voltage ramp and shape on the breakdown strength. In Fig. 4 e. g. the effect of different voltage signals used for breakdown testing can be seen. The breakdown strength of 1 mm thick Al_2O_3 and TiO_2 samples tested with a dc signal are (55.8 ± 3.5) kV/mm and (24.45 ± 7.2) kV/mm, respectively. As expected from literature (Ruemenapp and Peier, 1999), the breakdown strengths tested using dc signals are found to be higher compared to breakdown strengths tested using the rectified ac signal, with (35.58 ± 2.1) kV/mm for Al_2O_3 and (18.85 ± 3.4) kV/mm for TiO_2. But these are second order effects and have to be investigated in a second step in more detail.

Both Figs. 4 and 5 show that when the thickness d is reduced below the transition-thickness d_t a maximum materials specific breakdown strength E_{max} is reached.

Sun et al. (2012, 2013) calculated the breakdown strength of non-oxide ionic and covalently bonded materials with DFPT. The DFPT calculations were based on von Hippels electron avalanche model. The comparison of these calculated breakdown strengths with experimentally determined breakdown strengths for approx. 1µm thick films show good agreement. DFPT results for the materials in this study are not published. The avalanche model treats the dielectric breakdown as an intrinsic effect. As a consequence, it does not predict a thickness effect and is appropriate for $d < d_t$.

The thickness-dependence of the breakdown strength is often explained as Weibull effect similar to the mechanical case (Owate and Freer 1992, Malec et al. 2010). If a Weibull effect similar to the mechanical case were true, one is able to analyze the Weibull modulus from a plot of the breakdown strength as function of the sample thickness (for samples of constant electrode areas), which shows a slope of -1/2. In the mechanical case with these data the Weibull modulus can be analyzed to be m = 2 because the mechanical strength σ scales with the effective volume V_{eff} as $\frac{\sigma_1}{\sigma_2} = \left(\frac{V_{eff\,2}}{V_{eff\,1}}\right)^{1/m}$ (Munz and Fett 2001). In the case of the dielectric breakdown strength not exactly the same equation must hold, but one can draw the following conclusion. If all measured materials (ceramics and polymers) show the same thickness-dependence, it follows that they all should have the same defect distribution. This is highly unlikely and does not happen in the mechanical case. It would mean that all ceramic materials have the same Weibull modulus.

3.2. Permittivity-dependence of breakdown strength for ceramic materials

Besides the size-dependence the permittivity-dependence of the dielectric breakdown strength was evaluated. In Fig. 6 the experimental results of thin film measurements and 0.3 mm thick Al_2O_3, TiO_2, $SrTiO_3$ and $BaTiO_3$-samples are plotted as a function of the relative permittivity ε_r. The calculation of the theoretic breakdown strength E_{th}, which is also shown in Fig. 6, is explained in detail in the following chapter. With these four oxide ceramics a range of relative permittivities from 10 to 1000 could be covered.

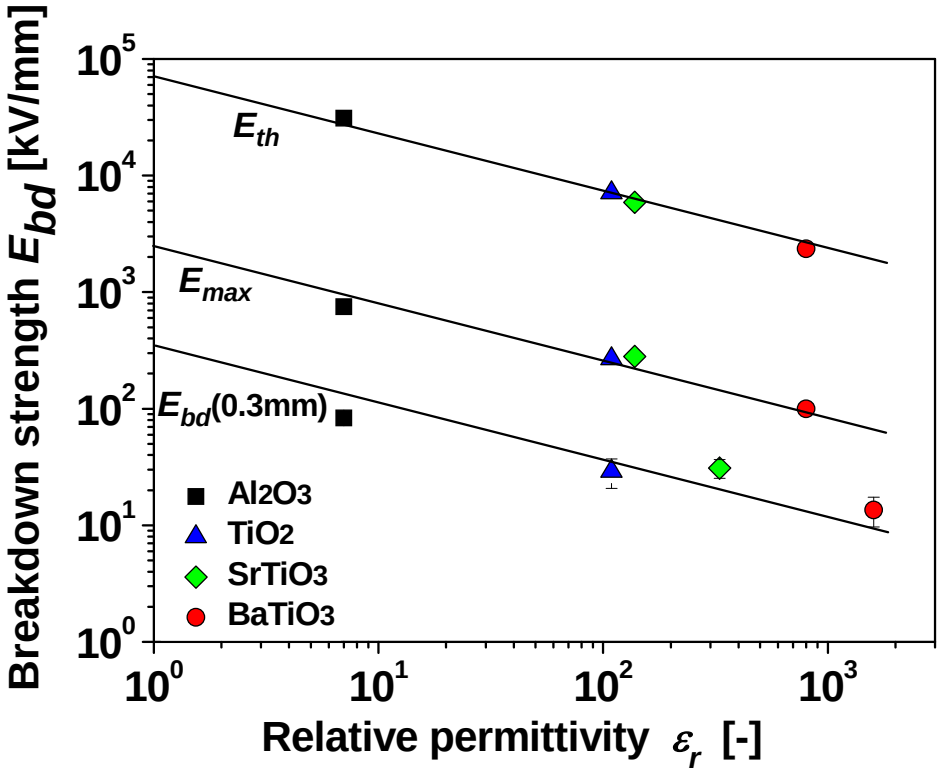

Fig. 6: Double logarithmic plot of dielectric breakdown strength E_{bd} versus the relative permittivity ε_r, for Al_2O_3, TiO_2 and $BaTiO_3$ polycrystalline samples and $SrTiO_3$ single crystals. E_{max} is calculated as mean value of the breakdown strengths from thin film data. E_{th} is calculated according to equation 7. The maximum breakdown strength E_{max} and the theoretical breakdown strength E_{th} for $SrTiO_3$ and $BaTiO_3$ are plotted versus relative permittivity values taken from literature sources (Baumert et al. 1997, Scott et al. 1994).

The $\frac{1}{\sqrt{\varepsilon_r}}$-dependence already studied for thin films (McPherson et al. 2002) is confirmed by the experimental data (E_{max}-values) for the intrinsic regime. Furthermore, our investigation shows that this is also true for the extrinsic regime ($E_{0.3mm}$-values) of ceramic materials. There is some scatter in the data which may be partly explained by the fact that the densities of the different materials were slightly different.

The relative permittivities of polymers are very close together, around 2, so their breakdown strengths do not allow an analysis of their permittivity-dependence.

3.3. Theoretical intrinsic breakdown strength

As mentioned in the introduction, the most recent DFPT-calculations by Sun et al. (2012, 2013) are very convincing. These calculations are physically based on an electron avalanche mechanism originally developed by von Hippel (1931a, b, 1932). In search of a simple intuitive model we think that Suo (1993) developed a nice physical approach, which is attractive to be presented and further developed. This breakdown model is based on models of the cleavage strength by Orowan (1949) and Polanyi (1921). In the following it will be shown that a further development of this model leads to the experimentally observed permittivity behavior. As an avalanche process needs a certain minimum sample thickness to develop, the following model might be the mechanism which leads to dielectric breakdown for samples, which are even not thick enough to develop an avalanche.

In analogy to the cleavage strength in fracture mechanics E_{max} is interpreted as intrinsic breakdown strength. Based on the ideas of Suo (1993), Orowan (1949) and Polanyi (1921) a simple intuitive theoretical model for the intrinsic or theoretical breakdown strength E_{th} is presented.

Suo (1993) assumes that for a perfect cubic dielectric crystal the electric field E to displace the electrons, which contribute to the polarization, is

$$E = E_{th} \sin\left(\frac{2\pi x}{2\lambda}\right) \qquad (1)$$

with E_{th} the theoretical breakdown strength, x the displacement distance due to applied electric field and λ a certain distance. Unlike Suo (1993) the spacing λ is not identified with the equilibrium lattice distance, instead, it will be determined. Additionally, not only the displacement of electrons but the displacement of charges relative to each other is assumed. As a consequence the model describes electronic and ionic polarization.

If q is the charge per unit volume, which contributes to the polarization, the polarization P is $\frac{qx}{b_0^3}$ with b_0 as the equilibrium spacing distance of the unit volume. For small $\frac{x}{b_0}$, the polarization P is proportional to the applied electric field E:

$$P = \frac{qx}{b_0^3} = \chi E \qquad (2)$$

with the electric susceptibility χ. As for small x the approximation $\sin(x) = x$ is valid, the theoretical breakdown strength E_{th} can be written for small x as

$$E_{th} = \frac{q\lambda}{\pi b_0^3 \chi} \qquad (3).$$

It is assumed that a dielectric breakdown leads to a complete destruction of the lattice. Hence, the energy γ to displace charges until the bond is completely destroyed is

$$\int_{x=0}^{\lambda} qE dx = q \int_{x=0}^{\lambda} E_{th} \sin\left(\frac{2\pi x}{2\lambda}\right) dx = \frac{2qE_{th}\lambda}{\pi} = \gamma \qquad (4)$$

and therefore the spacing λ can be expressed as

$$\lambda = \frac{\pi\gamma}{2E_{th}q} \qquad (5)$$

Eq. (5) introduced into Eq. (3) finally gives

$$E_{th} = \sqrt{\frac{\gamma}{2b_0^3\chi}} \approx \sqrt{\frac{\gamma}{2b_0^3\varepsilon_r\varepsilon_0}} \qquad (6)$$

for the theoretical breakdown strength. For materials with high susceptibilities $\chi = (\varepsilon_r - 1)\varepsilon_0 \approx \varepsilon_r\varepsilon_0$ it follows the same permittivity-dependence as shown in Fig. 6.

Physically the model compares the electrically stored energy density at breakdown $\varepsilon \cdot E_{th}^2$ with the energy to destroy the bond per volume γ / b_0^3.

As usually polymers and ceramics are multi-element materials, the energy γ to destroy the bond is approximated by the cohesive energy and the corresponding result for the theoretical breakdown strength is:

$$E_{th} = \sqrt{\frac{E_{coh} \cdot N_A \cdot \rho}{2M_{mol}\varepsilon_r\varepsilon_0}} \qquad (7)$$

with E_{coh} as cohesive energy, N_A as Avogadro constant, M_{mol} as molar mass of the compound and ρ as density.

The values for the cohesive energies, densities and relative permittivities are given in Table 4. The result of Eq. (7) applied to the investigated ceramic thin films predicts the measured permittivity-dependence as shown in Fig. 6 but overestimates the intrinsic breakdown strength E_{max}. This is probably attributed to the simplicity of the model, which includes the whole cohesive energy for the calculation, although it is unknown whether the complete lattice needs to be destroyed for dielectric breakdown. But the model may serve to estimate the maximum possible intrinsic breakdown strength E_{th}.

Tab. 4: Data used for calculation of the theoretical breakdown strength E_{th}.

	ρ [kg/m³]	ε_r [-]	E_{coh} [eV]	E_{th} [kV/mm]
Al_2O_3	3980 [1]	7	31.76 [5]	31048
TiO_2	4060 [1]	109	19.9 [6]	7105
$SrTiO_3$	5130 [2]	138 [3]	31.7 [7]	5911
$BaTiO_3$	6020 [2]	800 [4]	31.57 [8]	2354

[1] (Hellweg K., Hellweg A., 1975)

[2] (Hellweg K., Hellweg A., 1981)

[3] (Baumert et al., 1997)

[4] (Scott et al. 1994)

[5] (Urusov V.S., Eremin N. N., 1997)

[6] (Lazzeri, M., et al. 2001)

[7] (Ricci et al. 2003)

[8] (Erhart and Albe 2007)

3.4. Breakdown toughness and transition-thickness

Recently Schneider (2013) developed a theoretical breakdown model based on the assumption that out of a surface distribution of tiny, conducting filaments the longest will grow, when the dielectric breakdown strength E_{bd} is reached. This model is similar to the treatment of electrically conducting cracks in dielectrics and ferroelectrics (McMeeking 1990, Pak 1990, Heyer et al. 1998, Wang and Zhang 2001, Zhang and Gao 2004, Gehrig et al. 2008). The difference to existing models for conducting cracks and the 1D tubular breakdown models (Suo 1993, Beom and Kim 2008, Lin et al. 2009) is that space charge conductivity is introduced. Talbi et al. (2007) showed very nicely for alumina samples that dielectric breakdown occurs in the space charge regime, which is confirmed by our own unpublished results. Therefore, the Griffith type energy release rate model by Schneider (2013) includes space charge injection. It gives an expression for the extrinsic dielectric breakdown strength:

$$E_{bd} = \frac{1}{c}\sqrt{\frac{6}{5\pi}}\sqrt{\frac{G_{bd}}{\varepsilon_r \varepsilon_0}}\frac{1}{\sqrt{d}}\frac{1}{\sqrt{a_{bd}}} \qquad (8)$$

with G_{bd} as dielectric breakdown toughness, ε_r as relative permittivity of the dielectric and ε_o as permittivity of free space, d as sample thickness, a_{bd} the conducting filament-length and

$c \approx \sqrt{0.15}$. Eq. (8) predicts the measured thickness- and permittivity-dependence (see Figs. 4 - 6) in the extrinsic regime correctly and gives confidence that its physical assumptions are correct. It is based on the idea of a critical energy release rate or dielectric breakdown toughness G_{bd} necessary to initiate the unstable growth of the longest conducting filament in the sample surface. This dielectric breakdown toughness can be expressed as (Schneider 2013)

$$G_{bd} = \frac{5\pi c^2}{6} \varepsilon_r \varepsilon_0 a_{bd} d E_{bd}^2 \qquad (9)$$

The transition from the extrinsic to the intrinsic breakdown regime offers the possibility to determine the dielectric breakdown toughness. With the assumption of tiny, tubular conducting filaments it can be concluded that these filaments are typically shorter than the transition-thickness that means < 20 µm for ceramics and < 100 µm for polymers. Secondly if the filaments are tiny channels, their diameter should be at least 10 times smaller. As the transition-thickness is an upper estimate for the conducting filament-length, a_{bd} is approximated by $d_t/5$ at

$E_{bd} = E_{max}$.

Hence, the breakdown toughness can be calculated as:

$$G_{bd} = \frac{\pi c^2}{6} \varepsilon_r \varepsilon_0 d_t^2 E_{\max}^2 \qquad (10)$$

For the calculation of the breakdown toughness a transition-thickness d_t between 1–20 µm for $BaTiO_3$, TiO_2 and Al_2O_3 is used. The relative permittivities ε_r are taken from the sample characterization (Table 2), whereas the maximum breakdown strength E_{max} is evaluated as mean value in the thickness range < d_t from Fig. 4 with 804 kV/mm for Al_2O_3, 270 kV/mm for TiO_2 and 97 kV/mm for $BaTiO_3$. Applying Eq. 10, the breakdown toughness G_{bd} is calculated to be 3 - 1259 µJ/m for Al_2O_3, 6 - 2210 µJ/m for TiO_2 and 11 - 4217 µJ/m for $BaTiO_3$. The large intervals of the G_{bd}-values stem from the great uncertainty in d_t, which is squarely included. For polymer samples the data bases for PVC and PE samples is not sufficient for further calculation, therefore, only PMMA and PS were used to calculate the breakdown toughness G_{bd}. Here, a transition-thickness d_t between 10 - 100 µm is used for the calculation. The relative permittivity for PMMA and PS are taken from literature (Table 5), whereas the maximum breakdown strength E_{max} is evaluated as mean value in the thickness range < 10 µm from Fig. 5 with 311 kV/mm for PMMA and 407 kV/mm for PS. Applying Eq. 10, the breakdown toughness G_{bd} is calculated to be 18 - 1749 µJ/m for PMMA and 29 -

2880 µJ/m for PS. These breakdown toughness values for the ceramics and polymers are first estimations as the transition-thickness d_t is not determined very precisely.

The permittivities enter linearly in the 1D-toughness calculation (Eq. 10) but also in the toughness calculation given by Lin et al. (2009). Therefore, as $BaTiO_3$ and PZT have similar permittivities, we compare the 1D-toughness results for these two ceramics once determined in this study and by Lin et al. (2009). For the PZT ceramic PZT807 Lin et al. (2009) determine a value of 0.01-0.03 J/m which is a factor of 3 beyond the upper limit of our estimate for $BaTiO_3$ (0.004 J/m). In regard to the uncertainty of the transition-thickness as well as the estimate of the filament-length from the transition-thickness, this difference is acceptable. Additional experiments also with well-defined starter filaments are needed to determine the 1D-breakdown toughness more precisely.

Fu et al. (2000), Wang and Zhang (2001) determined a 2D-breakdown toughness for PZT ceramics. They showed that independent of the initial notch length a 2D-breakdown toughness of 223 J/m^2 can be determined for unpoled PZT-4-ceramics. This value is approx. 25 times larger than the measured mechanical toughness of this material. As this dielectric toughness is a 2D-toughness, it is difficult to compare it with a 1D-toughness.

3.5 Calculation of breakdown channel radius r_{bd}

The dielectric breakdown toughness G_{bd} is interpreted as the energy required for the initiation and growth of the breakdown channel by evaporating the material. An evaporation process due to heating is assumed because investigations of the breakdown channel show tubular holes with melted borders (Chao et al. 2010, Neusel et al. 2012, and Tunkasiri and Rujijanagul 1996). The breakdown channel is approximated as a cylindrical tube with constant radius r_{bd}. The thermal energy per channel length Q/a, which is required to create the breakdown channel, is calculated for the ceramic materials as follows

$$\frac{Q}{a} = \pi \cdot r_{bd}^2 \cdot \frac{E_{coh} \cdot N_A \cdot \rho}{M_{mol}} \qquad (11a)$$

with E_{coh} the cohesive energy, M_{mol} the molar mass of the compound, N_A the Avogadro constant and ρ the density of the material. For the amorphous polymers it is used

$$\frac{Q}{a} = \rho \cdot \pi \cdot r_{bd}^2 \cdot c_p \cdot \left(T_{dec} - T_0\right) \qquad (11b)$$

with ρ the density of the material, c_p the specific heat capacity, T_{dec} and T_o as decomposition and room temperature.

If the thermal energy per channel length Q/a is set to be equal to the breakdown toughness G_{bd}, the radius of the breakdown channel r_{bd} can be determined as

$$r_{bd} = \sqrt{\frac{G_{bd} M_{mol}}{\pi \cdot N_A \cdot \rho \cdot E_{coh}}} \qquad (12a)$$

for the ceramics and for the polymers:

$$r_{bd} = \sqrt{\frac{G_{bd}}{\rho \cdot \pi \cdot c_p \cdot (T_{dec} - T_0)}} \qquad (12b).$$

In Tables 4, 5 and 6 the data to calculate the breakdown channel radius r_{bd} and the resulting channel radii for polymer and ceramic samples are given.

Tab. 5: Data used for calculation of the channel radius r_{bd} of PMMA and PS.

	ρ [kg/m³]	**c_p** [J/kgK]	**T_{dec}** [K]	**ε_r** [-]	**E_{max}** [kV/mm]	**G_{bd}** [µJ/m]	**r_{bd}** [µm]
PMMA	1190 [9]	1465 [9]	603 [9]	2.6 [9]	311	17 - 1749	0.1 - 1
PS	1040 [10]	1210 [10]	633 [9]	2.5 [10]	407	28 - 2880	0.14 - 1.4

[9] (Vieweg, Esser 1975)

[10] (Becker, Braun, 1996)

Tab. 6: Data used for calculation of the channel radius r_{bd} of ceramic samples.

	E_{max} [kV/mm]	**G_{bd}** [µJ/m]	**r_{bd}** [µm]
Al_2O_3	804	3 - 1259	0.003 - 0.06
TiO_2	270	6 - 2210	0.004 - 0.09
$BaTiO_3$	97	11 - 4217	0.007 - 0.13

With the already determined values of the dielectric breakdown toughness the channel radii were calculated to be 0.003 - 0.06 µm for Al_2O_3, 0.004 - 0.09 µm for TiO_2 and 0.007 - 0.13 µm for $BaTiO_3$. The values are lower compared to radii reported in literature, which are in the range of 10 - 25 µm for ceramics and polymers (Budenstein 1980, Chao et al. 2010, Neusel et al. 2012, and Tunkasiri and Rujijanagul 1996). This difference is explained as follows. Breakdown tests in the extrinsic, size-dependent regime usually need high voltages. When the breakdown is initiated the high voltage source cannot be shut down fast enough to avoid additional current flow through the breakdown channel. This additional current leads to

additional evaporation and melting and results in a bigger channel radius than at the initial breakdown. In addition, dissipating processes nearby the channel are not taken into account. The radii for the polymer samples are calculated as 0.1 - 1 µm for PMMA and PS. According to Fothergill (1991), who calculated the filament-radius of PE to be 0.29µm, this is comparable to the dimensions of the gross morphology of polymer films.

3.6 Master curve of dielectric breakdown strength for ceramic materials

With the assumption that the length of the conducting filament is independent of the sample thickness d it follows by introducing Eq. (10) in Eq. (8)

$$E_{bd} = E_{\max}\sqrt{\frac{d_t}{d}} \qquad (13).$$

In Fig. 7 the experimentally measured breakdown strength E_{bd} of 0.3 mm and 1 mm thick samples are plotted versus E_{max} taken from Fig. 4. For both thicknesses it can be seen that E_{bd} shows an approximately linear relation to E_{max}.

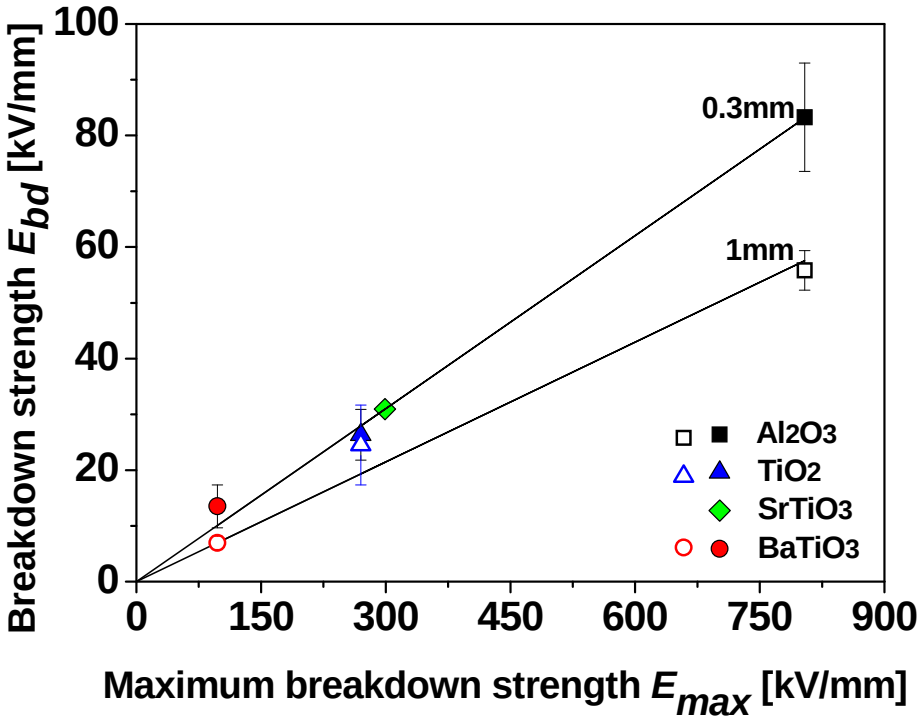

Fig. 7: Diagram of measured breakdown strength E_{bd} of 0.3 and 1 mm thick samples versus the maximum breakdown strength E_{max} (calculated as mean value from constant breakdown strengths of Fig. 4). The indicated lines are a linear fits with a slope of 0.103 for 0.3 mm thick samples and a slope of 0.072 for 1 mm thick samples.

Hence, it follows that d_t must be more or less constant for different ceramic materials. From the linear fits of Fig. 7 d_t is calculated to be 3 µm for the 0.3 mm thick samples and 5 µm for the 1 mm thick samples. The mean value of the calculated thicknesses 4 µm can be interpreted as a mean value of the transition-thickness range from Fig. 4. If this result is generally true, Fig. 7 can be used as a master curve to easily determine the maximum breakdown strength of thin films from bulk measurements or vice versa.

Moreover, from Fig. 6 it is possible to get the maximum intrinsic breakdown strength E_0 with 2.2 MV/mm by extrapolating the E_{max}-curve to a relative permittivity of 1. With the maximum intrinsic breakdown strength E_0 Eq. (13) can be written as:

$$E_{bd} = \frac{E_0}{\sqrt{\varepsilon}} \sqrt{\frac{d_t}{d}} \qquad (14)$$

with d_t as mean transition-thickness of 4 µm.

Based on Eq. (14) a "design"-map for dielectric breakdown strength with the variables of relative permittivity and sample thickness can be plotted (Fig. 8). According to the sample thickness and relative permittivity, it is now possible to determine the maximum dc field which can be applied.

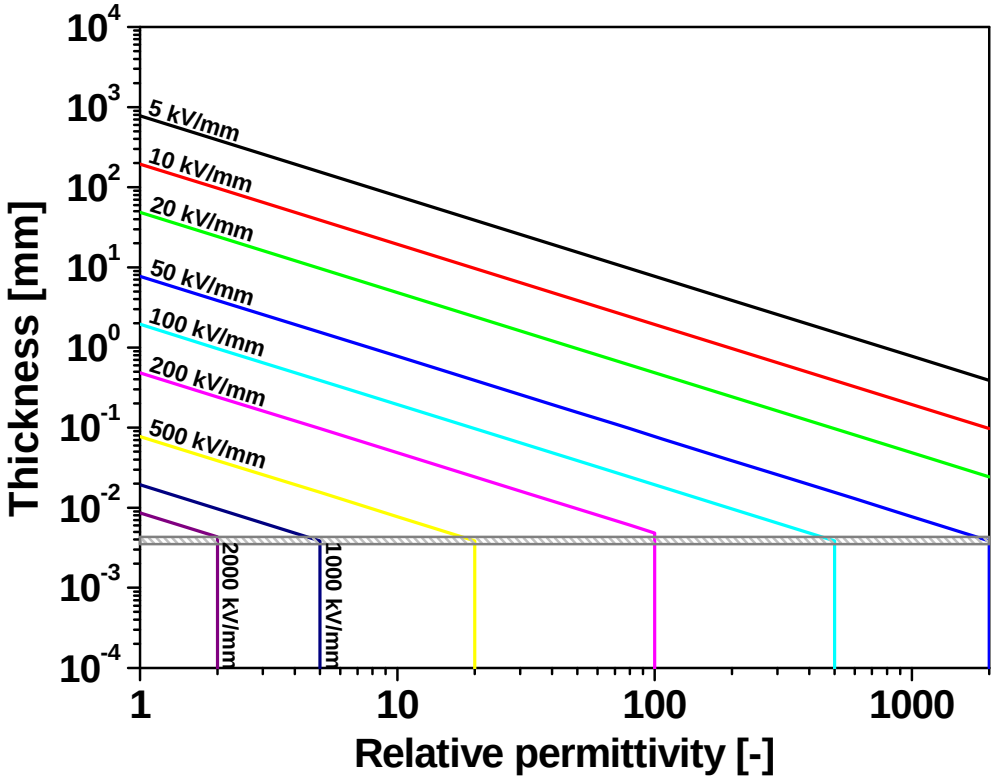

Fig. 8: "Design"-map of the dielectric breakdown strength as a function of sample thickness and relative permittivity calculated according to Eq. (14).

4. Conclusions

The thickness-dependence of the extrinsic dielectric breakdown strength scales as $\frac{1}{\sqrt{d}}$ down to the micrometer scale. Below a materials dependent transition-thickness a roughly thickness-independent intrinsic dielectric breakdown regime exists. The investigations demonstrate that the $\frac{1}{\sqrt{\varepsilon_r}}$-dependence of the dielectric breakdown strength for ceramic materials is thickness-independent. All these results strongly support the idea that in the extrinsic breakdown regime conducting surface-filaments exist, which initiate breakdown. Therefore, future research should be directed towards a validation of an energy release rate based breakdown model and the experimental determination of the dielectric breakdown toughness G_{bd} by introducing tiny, conducting filaments. This would allow characterising the dielectric breakdown behaviour not only in terms of the breakdown strength but also in terms of the dielectric breakdown toughness. Finally the physical nature of the initial conducting filaments must be determined in order to be able to tailor the chemistry and microstructure of dielectric materials for better dielectric breakdown resistance. All these investigations open new space for a novel "dielectric breakdown electrics" research area.

Acknowledgements

The authors gratefully acknowledge financial support by the German Research Foundation (DFG) under Project number SCHN-372/17-1. We thank Dieter Schmidt and Hans Jelitto for their assistance during ac breakdown measurements. We thank Manfred Eich allowing us to use their clean room and spin-coating equipment and Zied Fahem for his advices concerning the polymer thin-film preparation.

References

Baumert, B. A., Chang L.-H., Matsuda A. T., Tsai T.-L., Tracy C. J., Gregory R. B., Fejes P. L., Cave N. G., Chenet W., 1997. Characterization of sputtered barium strontium titanate and strontium titanate-thin films. J. Appl. Phys. 82, 2558-2566.

Becker, G.W., Braun, D., 1996. Kunststoff-Handbuch 4., Hanser Verlag, München.

Beom, H. G., Kim, Y. H., 2008. Application of *J* integral to breakdown analysis of a dielectric material. Int. J. Solids Struct. 45, 6045–6055.

Brehmer L., Eberhardt M., Konietzko K. D., Böhm J., Röhr L., Lerch C., Winkler H., 1983. Elektrische Eigenschaften polymerer Festkörper–Physikalische Grundlagen und technische Anwendungen. Teil II. Polymere Isolatoren und Dielektrika. Acta Polym. 34, 287–298.

Budenstein P. P., 1980. On the mechanism of dielectric breakdown of solids. IEEE Trans. Electr. Insul. EI-15, 225-240.

Campbell, S. A., Gilmer D. C., Wang X.-C., Hsieh M.-T., Kim H.-S., Gladfelter W. L., Yan J., 1997. MOSFET transistors fabricated with high permittivity TiO_2 dielectrics. IEEE Trans. Electron Devices 44, 104-108.

Castro, P., Buchenauer, C.J., Gaudet, J., Schamiloglu, E., 2005. Studies of dielectric breakdown under pulsed power conditions. IEEE Pulsed Power Conference. pp. 978-981.

Chao, S., Petrovsky, V., Dogan, F., 2010. Effects of sintering temperature on the microstructure and dielectric properties of titanium dioxide ceramics. J. Mater. Sci. 45, 6685-6693.

Chin, A., Wu, Y.H., Chen, S.B., Liao, C.C., Chen, W.J., 2000. High quality La_2O_3 and Al_2O_3 gate dielectrics with equivalent oxide thickness 5-10 Å. Symposium on VLSI Technology. Digest of Technical Papers.

De Wit H.J., Crevecoeur C., 1974. The dielectric breakdown of anodic aluminum oxide. Phys. Lett. 50 A, 365-366.

Dissado, L. A., Fothergill J. C., 1992. Electrical degradation and breakdown in polymers, part 2. Peter Peregrinus Ltd., London, pp.69-74.

Erhart, P., Albe, K., 2007. Thermodynamics of mono- and di-vacancies in barium titanate. J. Appl. Phys. 102, 0841111-0841118.

Fock, V., 1927. Zur Wärmetheorie des elektrischen Durchschlags. Archiv f. Elek. 19, 71-81.

Fothergill, J. C., 1991. Filamentary electromechanical breakdown. IEEE Transactions on Electrical Insulation. 26, 1124-1129.

Fröhlich, H. 1939. Dielectric breakdown in solids. Rep. Prog. Phys. 6, 411-430.

Fu, R., Qian, C.-F., Zhang, T.-Y., 2000. Electrical fracture toughness for conductive cracks driven by electric fields in piezoelectric materials. Appl. Phys. Lett. 76, 126-128.

Gao, H., Ji, B., Jäger I. L., Arzt E., Fratzl P., 2003. Materials become insensitive to flaws at nanoscale: lessons from nature. PNAS 100:10, 5597–5600.
Gehrig, F., Jelitto, H., Schneider G.A., 2008. Fracture criterion for a conducting crack in poled PZT-PIC 151 investigated by stable crack growth. Acta Mater. 56, 222–229.
Hellwege, K.-H., Hellwege A.M., 1975. Landolt-Börnstein, Crystal structure data of inorganic compounds. 7 b, Springer Verlag, Berlin.
Hellwege, K.-H., Hellwege, A.M., 1981. Landolt-Börnstein, Ferroelectrics and related systems. 16, Springer Verlag, Berlin.
Heyer, V., Schneider, G.A., Balke, H., Drescher, J., Bahr, H.-A., 1998. A fracture criterion for conducting cracks in homogeneously poled piezoelectric PZT-PIC 151 ceramics. Acta Mater. 46, 6615-6622.
Ieda, M., Nagao, M., Hikita, M., 1994. High-field conduction and breakdown in insulating polymers. Present situation and future prospects. IEEE Trans. Dielectr. Electr. Insul. 1, 934-945.
Joffé, A. F., 1927. Mechanical and electrical strength and cohesion. Trans. Faraday Soc. 24, 65-72.
Jow, J.R., Cygan, P.J., 1993.Dielectric breakdown of polyvinylidene fluoride and its comparisons with other polymers. J. Appl. Phys. 73, 5147-5151.
Kim, H.-S., Gilmer, D. C., Campbell, S. A., Polla, D. L., 1996. Leakage current and electrical breakdown in metal-organic chemical vapor deposited TiO_2 dielectrics on silicon substrates. Appl. Phys. Lett. 69, 3860-3862.
Klein, N., Gafni, H., 1966. The maximum dielectric strength of thin silicon oxide films. IEEE Trans. Electron. Devices.13, 281-289.
Kolodzey, J., Chowdhury E. A., Thomas A. N., Qui G, Rau I., Olowolafe J. O., Suehle J. S., Chen Y., 2000. Electrical conduction and dielectric breakdown in aluminum oxide insulators on silicon. IEEE Trans. Electron Devices 47, 121-128.
Lazzeri, M., Vittadini, A., Selloni, A., 2001. Structure and energetics of stoichiometric TiO_2 anatase surfaces. Phys. Rev. B. 63, 155409, 1-9.
Li, W.-T., McKenzie, D. R., McFall, W. D., Zhang, Q.-C., Wiszniewski, W., 2000. Breakdown mechanism of Al_2O_3 based metal-to-metal antifuses. Solid-State Electron. 44, 1557-1562.
Lin, S., Beom, H. G., Tao, D., Kim, Y. H., 2009. Dielectric breakdown of an unpoled piezoelectric material with a conductive channel. Fatigue Fract. Eng. Mater. Struct. 32, 580-586.
Lee, B.H., Jeon Y., Zawadzki K., Qi W.-J., Lee J., 1999. Effects of interfacial layer growth on the electrical characteristics on thin titanium oxide films on silicon. Appl. Phys. Lett. 74, 3143-3145.

Malec, D., Bley, V., Talbi, F., Lalam, F., 2010. Contribution to the understanding of the relationship between mechanical and dielectric strength of alumina. J. Eur. Ceram. Soc. 30, 3117-3123.
McMeeking, R. M., 1986. On mechanical stresses at cracks in dielectrics with supplication to dielectric breakdown. J. Appl. Phys. 62, 3116-3122.
McMeeking, R. M., 1990. A J-integral for the analysis of electrically induced mechanical stress at cracks in elastic dielectrics. Int. J. Eng. Sci. 28, 605-613.
McPherson, J., Kim, J., Shanware, A., Mogul, H., Rodriguez, J., 2002. Proposed universal relationship between dielectric breakdown and dielectric constant. International Electron Devices Meeting. IEDM '02, pp. 633-636.
Milliken, A.D., Bell, A.J., Scott, J.F., 2007. Dependence of breakdown field on dielectric (interelectrode) thickness in base-metal electrode multilayer capacitors. Appl. Phys. Lett. 90, 112910-112913.
Miyairi, K., Itoh, E., 2004. AC electrical breakdown and conduction in PMMA thin films and the influence of $LiClO_4$ as an ionic impurity. Proc. ICSD 1, 99-102.
Moon, P. H., 1931. The theory of thermal breakdown of solid dielectrics. In: Proceedings of the North Eastern District Meeting of the A.I.E.E. pp. 1008-1021.
Munz, D., Fett, T., 2001. Ceramics mechanical properties, failure behavior, materials section. In: Hull, R., Osgood Jr., R. M., Sakaki, H., Zunger, A. editors, Springer Series in Material Science 36. Springer-Verlag Berlin.
Nagao, M., Kosaki, M., Mizuno, Y., 1992. On temperature dependence of electric strengths of polar polymeric films in low-temperature region. Sixth International Conference on Dielectric Materials, Measurements and Applications. pp. 85-88.
Nafría, M., Suñé, J., Aymerich, X., 1996. Breakdown of thin gate silicon dioxide films—A review. Microelectronics Reliability. 36, 871-905.
Neusel, C., Jelitto, H., Schmidt, D., Janssen, R., Felten, F., Schneider, G.A., 2012. Dielectric breakdown of alumina single crystals. J. Eur. Ceram. Soc. 32, 1053-1057.
Oakes, W.G., 1948. The intrinsic electric strength of polythene and its variation with temperature. J. Inst. Electr. Eng. Part I: Gen., 95, 36-44.
O'Dwyer, J.J., 1958. Dielectric breakdown in solids. Adv. Phys. 7, 349-394.
O'Dwyer, J.J., 1967. The theory of avalanche breakdown in solid dielectrics. J. Phys. Chem. Solids 28, 1137-1144.
O'Dwyer, J.J., 1982. Breakdown in solid dielectrics. IEEE Trans. Electr. Insul. EI-17, 484-487.
Orowan, E., 1949. Fracture and strength of solids. Rep. Prog. Phys. 12, 183-232.

Owate, I.O., Freer, R., 1988. The dielectric breakdown of alpha alumina ceramic at room temperature. Sci. Ceram. 14, 1013-1018.
Owate, I.O., Freer, R., 1989. The ac electrical breakdown of some aluminum nitride ceramics. Silic. Ind. 7-8, 123-127.
Owate, I.O., Freer, R., 1990. The electrical properties of some cordierite glass ceramics in the system $MgO\text{-}Al_2O_3–SiO_2–TiO_2$. J. Mater. Sci. 25, 5291-5297.
Owate, I.O., Freer, R., 1991. Solidification structures on alumina ceramics and cordierite glass-ceramics after dielectric breakdown. Proc. Brit. Ceram. Soc. 48, 25-34.
Owate, I. O., Freer, R., 1992. Dielectric breakdown of ceramics and glass ceramics. Sixth International Conference on Dielectric Materials, Measurements and Applications. pp. 443-446.
Pak, Y. E., 1990. Crack extension force in a piezoelectric material. J. Appl. Mech. 57, 647-653.
Park, D.-G., Cho, H.-J., Lim, K.-Y., Lim, C., Yeo, I.-S., Roh, J.-S., Park, J. W., 2001. Characteristics of n^+ polycrystalline-$Si/Al_2O_3/Si$ metal-oxide-semiconductor structures prepared by atomic layer chemical vapor deposition using $Al(CH_3)_3$ and H_2O vapor. J. Appl. Phys. 89, 6275-6280.
Polanyi, M., 1921. Über die Natur des Zerreißvorgangs. Z. Phys. 7, 323-327.
Ricci, D., Bano, G., Pacchioni, G., 2003. Electronic structure of a neutral oxygen vacancy in $SrTiO_3$. Phys. Rev. B. 68, 224105.
Ruemenapp, T., Peier, D., 1999. Dielectric breakdown in aluminum nitride. High Voltage Engineering Symposium, 467, 22-27.
Schneider, G.A., 2013. A Griffith type energy release rate model for dielectric breakdown under space charge limited conductivity. J. Mech. Phys. Solids. 61, 78–90.
Scott, J.F., Azuma M., Paz de Araujo C. A., McMillan L. D., Scott M. C., Roberts T., 1994. Dielectric breakdown in high-ε films for ULSI DRAMs: II. Barium-strontium titanate ceramics. Integ. Ferroelec. 4, 61-84.
Stark, K. H., Garton, C. G., 1955. Electric strength of irradiated polythene. Nature. 176, 1225-1266.
Sun, Y., Boggs, S. A., Ramprasad, R., 2012. The intrinsic electrical breakdown strength of insulators from first principles. Appl. Phys. Lett. 101, 132906.
Sun, Y., Bealing, C., Boggs, S., Ramprasad, R., 2013. 50+ years of intrinsic breakdown. IEEE Electr. Insul. Mag. 29, 8-15.
Suo, Z., 1993. Models for breakdown-resistant dielectric and ferroelectric ceramics. J. Mech. Phys. Solids. 41, 1155-1176.

Talbi, F., Lalm, F., Malec, D., 2007. DC conduction of Al_2O_3 under high electric field. J. Phys. D: Appl. Phys. 40, 3803–3806.

Tunkasiri, T., Rujijanagul, G., 1996. Dielectric strength of fine grained barium titanate ceramics. J. Mater. Sci. Lett. 15, 1767-1769.

Urusov, V.S., Eremin, N. N., 1997. Charge–transfer energy in computer modeling of structure and properties of minerals. Phys. Chem. Miner. 24, 374-383.

Vieweg, R., Esser, F., 1975. Kunststoff-Handbuch. 9, Hanser Verlag, München.

Vojta, A., Clarke, D.R., 1998. Electric field singularity at an electrode tip in a nonlinear electrical conductor. J. Appl. Phys. 83, 5632–5635.

von Hippel, A., 1931a. Der Mechanismus des elektrischen Durchschlags in festen Isolatoren I. Z. Phys. 67, 707-724.

von Hippel, A., 1931b. Der Mechanismus des elektrischen Durchschlags in festen Isolatoren II. Z. Phys. 68, 309-324.

von Hippel, A., 1932. Der Mechanismus des elektrischen Durchschlags in festen Isolatoren III. Z. Phys. 75, 145-170.

Wagner, K. W., 1948. Der elektrische Durchschlag von festen Isolatoren. Archiv f. Elek. 39, 215-233.

Wang, T., Zhang, T.-Y., 2001. Electrical fracture toughness for electrically conductive deep notches driven by electric fields in depoled lead zirconate titanate ceramics. Appl. Phys. Lett. 79, 4198-4200.

Zeller, H. R., Schneider, W. R., 1984. Electrofracture mechanics of dielectric aging. J. Appl. Phys. 56, 455-459.

Zhang, T.Y., Gao, C.F., 2004. Fracture behaviors of piezoelectric materials. Theor. Appl. Fract. Mech. 41, 339-379.